Structural complexity of the intermetallic compound *o*-$Al_{13}Co_4$

Paul Simon[1], Iryna Zelenina[1], Reiner Ramlau[1], Wilder Carrillo-Cabrera[1], Ulrich Burkhardt[1], Horst Borrmann[1], Raul Cardoso Gil[1], Michael Feuerbacher[2], Peter Gille[3], Yuri Grin[1*]

[1]*Max-Planck-Institut für Chemische Physik fester Stoffe, Nöthnitzer Str. 40, 01187 Dresden, Germany*

[2] *Peter-Grünberg-Institut, Forschungszentrum Jülich GmbH, 52425 Jülich, Germany*

[3]*Ludwig-Maximilians-Universität München, Department of Earth and Environmental Sciences, Crystallography Section, Theresienstr. 41, 80333 München, Germany*

ABSTRACT

The crystal structure of the complex intermetallic phase *o*-$Al_{13}Co_4$ was first investigated 1994, but some open questions still remained. The new refinement of the crystal structure using high-resolution X-ray diffraction data resulted in a much more complex model including a large number of split positions (space group $Pnm2_1$, a = 8.1590(6), b = 12.349(1), c = 14.453(1) Å). The model is interpreted in terms of local violation of the translational symmetry, which is confirmed by HRTEM and HRSTEM investigations. Chemical bonding between two partial structures in *o*-$Al_{13}Co_4$ - three-dimensional framework and linear Co-Al-Co groups in cages of the latter - and stacking faults (local twinning) are discussed as possible reasons for such extended disorder.

KEYWORDS

o-$Al_{13}Co_4$ ×intermetallic compound ×disorder ×structural complexity ×quasicrystal approximant ×chemical bonding ×TEM × STEM ×single-crystal X-ray diffraction

*Corresponding author. E-mail: grin@cpfs.mpg.de; Phone: +49-351-4646 4000; Fax: +49-35-4646 4002

INTRODUCTION

Characteristic for the interaction of aluminum with the late transition metals, the aluminum-rich part of the system Al-Co [1-3] is very suitable for the formation of the binary phases. Numerous compounds with increasing complexity of crystal structures are reported in literature: AlCo (CsC1 type of crystal structure [4]), $A1_5Co_2$ (prototype structure [5,6]), Al_3Co, *o*-$Al_{13}Co_4$, *m*-$Al_{13}Co_4$, and Al_9Co_2 (prototype structure [7,8]). The region of the phase diagram around the composition Al_3Co is especially complex [9,10]. Beside specific bonding features of Al_5Co_2 [11], in particular the compound *o*-$Al_{13}Co_4$ recently attracted attention of several research groups because of its unusual physical and chemical properties. From a crystallographic point of view, this substance with more than 100 atoms in the unit cell is considered as so-called complex intermetallic compound (or complex metallic alloy, CMA [12]) and a quasicrystal approximant [13]. It exhibits strongly anisotropic magnetic and electronic transport behavior, *e.g.* depending on the crystallographic direction, the Seebeck coefficient changes from positive along [100] via close to zero one along [001] to negative along [010] [14]. Investigations on the structure of the (100) surface revealed atomic arrangements characteristic for site isolated catalytic centers [15,16]. This was a starting point to assume and to study catalytic activity of *o*-$Al_{13}Co_4$ in the semi-hydrogenation of acetylene. The properties appeared to be outperforming the industrial catalyst and, along with $Al_{13}Fe_4$, it was considered a low-cost alternative to palladium-containing catalysts [17].

In order to understand these striking features, information concerning the real structural organization of this material was on demand. First, the monoclinic phase *m*-$Al_{13}Co_4$ was investigated at the composition $Al_{73.66}Co_{26.34}$ [18]. In accordance with the homeotypism relationship, the structure type $Al_{13}Fe_4$ was assigned, despite obtained symmetry (space group *Cm*) and refined composition deviating from that of $Al_{13}Fe_4$. An orthorhombic unit cell (space group *Pnmn*) was later suggested for composition Al_3Co [19] but could not be confirmed afterwards. A similar orthorhombic crystal structure (space group $Pmn2_1$) was primarily refined at the composition $Al_{13}Co_4$, using single-crystal diffraction data (crystal 0 in Table 1) [20]. Besides the relatively large residual of ca. 6%, several aluminum positions showed extremely large atomic displacement parameters, which could be refined only in isotropic approximation indicating further crystallographic disorder. The quality and size of the available crystals did not allow for better resolution of the X-ray diffraction experiment [20]. The cobalt positions were clearly observed also by high-angle annular dark-field (HAADF) STEM investigations [21]. However, HAADF images do not provide sufficient information about the aluminum positions, as this technique is more sensitive to the higher atomic-number element cobalt. In

this paper, we report on a new attempt to clarify the crystal structure of orthorhombic *o*-$Al_{13}Co_4$ combining high-resolution single-crystal X-ray diffraction with spherical aberration corrected HRTEM and HRSTEM.

EXPERIMENTAL

Preparation

For diffraction experiments, small pieces of three centimeter-sized single crystals were used. The first one (crystal 1) was grown by the Bridgman method, two others – by the Czochralski technique (crystals 2 and 3). The details of the Czochralski experiment were already published [22]. For the Bridgman growth, pre-alloyed material of initial composition Al 84.5 at. %, Co 15.5 at. % was molten in a tapered boron-nitride crucible. The growth was performed under vacuum with a pulling speed of 0.5 mm h^{-1}. The grain sizes achieved were of the order of 1 cm^3. The quality of the material was characterized by phase-contrast optical microscopy, scanning electron microscopy, and transmission electron microscopy (TEM). The final composition of the crystal was 76.5 at. % Al and 23.5 at. % Co. The HRTEM and HRSTEM study was performed on crystal 2.

X-ray diffraction

X-ray powder diffraction patterns of parts of the single crystals were obtained with a Huber Imaging Plate Guinier Camera G670 using Co$K\alpha_1$ radiation (l = 1.788996 Å, 8 × 15 min scans, $6° \leq 2q \leq 100°$). Unit cell parameters were determined using the positions of 298 reflections extracted from powder diffraction pattern measured with LaB_6 as internal standard (a = 4.15692 Å).

Irregularly shaped crystals of *o*-$Al_{13}Co_4$ were isolated by careful mechanical treatment of the large single-crystalline specimens. Their quality was preliminarily checked and the intensity data collection was performed on a Rigaku R-Axis Spider diffraction system using Ag$K\alpha$ radiation (λ = 0.56081 Å) for crystals 1 and 2 or Rigaku AFC7 diffraction system equipped with a Saturn 724+ detector using Mo$K\alpha$ radiation (λ = 0.71073 Å) for crystal 3, respectively. An empirical absorption correction of the reflection intensities was performed. Relevant crystallographic information and details of data collection and handling are listed in Table 1. As the obtained atomic coordinates are equal for all three crystals within a few estimated

standard deviations, the final values of atomic parameters are presented only for crystals 1 and 2 manufactured by different techniques, respectively (Table 2).

Transmission electron microscopy

For TEM investigations, focused ion beam (FIB) thin cuts of crystal 2 were prepared with a FEI Quanta 200 3D dual beam device (FEI, Eindhoven, Netherlands) with cuts parallel to (100) and (010) planes. These oriented lamellae were transferred onto a molybdenum half ring. The selected region was covered with a protective layer of platinum (thickness 1–2 µm, acceleration voltage 30 kV and current 0.3 nA). After this preparation, the particles were thinned down to electron transparency (thickness of 100–200 nm) in the FIB system at 30 kV acceleration voltage, currents of 3.0 – 0.05 nA for the Ga^+-ion beam.

The lowest thickness was about 200 nm as further FIB thinning of the lamella destroyed the material. Moreover, FIB thinning below this critical thickness led to bending of the lamella. The lamellae were further polished by a mild argon-ion stream at lower energies in order to obtain even thinner samples. In addition, in this way it is possible to polish away amorphous layers caused by gallium milling and to remove Ga implantations from the surface. Subsequently, argon polishing was performed (PIPS model 691 device, Gatan Inc., Pleasanton, CA, USA). Liquid-nitrogen cooling and application of low voltage (2.5-0.2 kV) helped to get thin wedge shaped lamellae for HRTEM with reduced Ga content. However, the range around ion energy of 1 kV was avoided, as Ar-beam knock-on damage was observed at that energy.

Spherical-aberration corrected high-resolution TEM (HRTEM) and scanning TEM (HRSTEM) analyses of the sample were performed with JEM-ARM300F microscope (Grand ARM, JEOL, Akishima, Japan) with double correction. Dodecapole correctors in the beam and the image forming system correct the spherical aberration of the condenser and the objective lenses, respectively. TEM resolution is 0.5 - 0.7 Å depending on resolution criterion applied, STEM resolution is 0.5 Å. TEM images were recorded on a 4k × 4k pixel CCD array (Gatan US4000). Additional analysis was carried using a FEI Tecnai F30-G2 with Super-Twin lens (FEI) with a field-emission gun at an acceleration voltage of 300 kV. The point resolution amounted to 2.0 Å, and the information limit amounted to about 1.2 Å. The microscope is equipped with a slow scan CCD camera (MultiScan, 2k×2k pixels; Gatan Inc., Pleasanton, CA, USA).

RESULTS AND DISCUSSION

The lattice parameters of *o*-$Al_{13}Co_4$ were obtained from indexing of the single crystal X-ray diffraction data and confirmed by HRTEM experiments. Fast-Fourier transforms (FFT) of the

HRTEM images along the [100] and [010] directions (Fig. 1) do not reveal additional reflections indicating that the lattice parameters extracted from the X-ray diffraction data are correct. Analysis of the extinctions in the data set yields extinction symbol *P--n* with the possible space groups $Pmn2_1$ and *Pmmn*. An attempt of structure solution in the centrosymmetric space group *Pmmn* did not deliver reasonable results. The refinement of the structural model from Ref. [20] (space group $Pmn2_1$, 102 atoms in the unit cell, composition $Co_{24}Al_{78}$) in isotropic approximation of the atomic displacement parameters (ADP) resulted in $R_F = 0.073$. Already at this stage, a huge scattering of the ADPs, 0.0040 to 0.0104 Å^2 for cobalt and 0.0038 to 0.0475 Å^2 for aluminum atoms is observed. Application of the anisotropic approximation on the ADPs reduced the residual R_F to 0.038, but the atomic displacement turned out to be strongly anisotropic. In particular, several aluminum atoms located on the mirror planes (Wyckoff site 2*a* 0*yz*) revealed very large ratios $U_{22} >> U_{11} \approx U_{33}$ or $U_{33} >> U_{11} \approx U_{22}$. The difference electron density in the (100) plane calculated without those atoms which exhibit strong anisotropy of the ADPs ($R_F = 0.146$, Fig. 2) reveals a distribution around the omitted atomic positions which is far from spherical. The strong anisotropy of the ADPs – in particular multiple local maxima – points toward local occupancy disorder in the crystal structure. Indeed, several split positions were necessary to describe the electron density in those regions. The occupancy parameters of some split positions - where this was obvious from the analysis of interatomic distances - were constrained to unity, other occupancy parameters were refined without restrictions (Table 2). The final residual R_F dropped slightly to 0.035 (Table 1), and the anisotropy of the ADPs was markedly reduced. The refined compositions for three crystals 1-3 with ca 100 atoms per unit cell (Table 1) differ markedly to the ideal structure (no splits and no defects, 102 atoms per unit cell).

The interpretation of the obtained split model can be derived in the context of local disorder considering the interatomic distances. In the region containing atoms Al1, Al7, Al13 and Al26 atoms, the first position is partially occupied, and the other three split into two or three positions each (Fig. 3). All distances between the aluminum and cobalt atoms are larger than 2.23 Å, which is characteristic for all other Al-Co distances in this crystal structure. Al-Al distances larger than 2.3 Å can be obtained only in selected sets of neighboring positions, e.g., Al1-Al7-Al26a-Al13a, Al13-Al26b-Al7a or Al13a-Al26-Al7a, which indicates several ordered atomic arrangements in this part of the crystal structure. Moreover, they result in slightly different compositions being a reason for the deviation of the refined composition of the crystal structure from the ideal one $Al_{78}Co_{24}$.

In order to verify the assumption of local atomic disorder, the study was continued by means of high-resolution transmission electron microscopy. As the earlier TEM studies were carried out on single crystals of *o*-$Al_{13}Co_4$ manufactured by the Bridgman technique [23-26], single crystal 2 of *o*-$Al_{13}Co_4$ grown by the Czochralski technique [22] was now used for TEM investigations (Fig. 4a). Overview TEM images of the argon-polished FIB cuts (Fig. 4b) show bend/thickness contours and sharp steps indicating different sample thickness in different regions (Fig. 4c) in agreement with the observations of the surface studies [15,16].

Comparison with the structure model obtained from the X-ray diffraction data show that the main contrast features of the high-resolution TEM (HRTEM) micrograph along [100] direction are created by vertex- and edge-connected Co pentagons with side lengths of 4.72 - 4.95 Å (Fig. 5a). Within the large pentagon, a smaller-sized pentagon shows up with a side length of 2.75 – 3.05 Å formed exclusively by aluminum atoms. In the center of each of these double-pentagons, a column consisting of cobalt and aluminum atoms is situated. The aluminum atoms within the pentagons are disordered. They are shifted from the regular positions and do not reflect anymore the arrangement of the ordered structure. A variant of the complete disordered model with four removed Al atoms and one half-occupied Al position matches the image contrast within the pentagon of interest (Fig. 5b). The cobalt atoms at the corners of the pentagon should appear bright, however, the contrast of the central cobalt position and the positions at the corners is blurred, and the obtained intensity is lower compared to Al as observed in the HRSTEM micrographs (Fig. 6). For the selected Co-pentagon, the HRTEM image, the disordered model, the image simulation and the distribution of Coulomb potential are shown in Figs. 5c-f.

Spherical-aberration corrected scanning transmission electron microscopy (STEM) was performed in order to visualize quantitatively the difference between the ordered (Fig. 6a) and disordered (Fig. 6b) models of *o*-$Al_{13}Co_4$. The pentagonal arrangements of Co are clearly recognizable in the overview image of the [100] zone (Fig. 6c). Most impressive is the finding, that in every pentagon the Al atoms are differently ordered (Fig. 6c,d). It becomes obvious that even the Co atoms at certain positions at the corners of the pentagons appear to be absent (Fig. 6e,f). The weak Co intensity at these positions can be explained either by the zig-zag arrangement of Co along the viewing direction or by a lack of Co atoms in the column. The simulations show that the removal of as little as one Co of a column within the unit cell along the [100] direction explains the reduced intensity in the STEM image (Fig. 6g-i).

Deviations from the translational symmetry are also seen in the [010] zone in high-resolution TEM (Fig. 7), despite the structure model with all split positions (Fig. 7a) and the model of ordered structure (Fig. 7b) discern only subtle differences in this projection. In general, each of

the unit cells is slightly different because of the different split positions of aluminum and cobalt atoms within the central layer. Furthermore, additional interstitial atoms are observed between the layers (Fig. 7c,d). The Al atoms belonging to the Co-Al-Co groups are clearly identified (Fig. 7e,f).

According to the high-resolution X-ray single-crystal diffractions experiments, as well as the HRTEM and HRSTEM studies, the crystal structure of *o*-$Al_{13}Co_4$ is characterized by strong local deviations from translational symmetry in vicinity of the mirror planes. This allows to understand the deviation from the ideal composition $Al_{78}Co_{24}$. Moreover, the difficulties describing the structure in the centrosymmetric space group *Pmmn* and the non-reasonable values of 0.2-0.3 for the Flack parameter (for a non-centrosymmetric crystal structure in correct setting it is expected be close to zero [27,28], the obtained value points toward pseudo-inversion) by the description in the non-centrosymmetric space group $Pmn2_1$ (subgroup of *Pmmn*) are also ascribed to these local deviations.

Furthermore, averaging the coordinates of the split positions and optimizing them allows to generate an ordered model with the ideal composition. This model was found to be sufficient to understand the results from investigation of the atomic arrangements on the (100) surface [15,16], anisotropic magnetic and electronic transport properties [14], formation of the isolated active catalytic centers [17], results of the NMR investigations [29] and to perform chemical bonding analysis in this compound [12].

The quantum chemical calculations applying the positional space approach yields two partial structures in *o*-$Al_{13}Co_4$ (Fig. 8a). The main three-dimensional framework is formed by Al-Al and Al-Co interactions and shows cavities bearing the three-atomic Co-Al-Co groups bonded by two-center Co-Al interactions. Both partial structures interact by multi-center bonds. The cavities have the shape of pentagonal prisms capped on both basal sides by pentagonal antiprisms. The basal faces of the latter are strongly deformed, so that three of five possible vertices form triangular caps of the cages with two others being shifted apart (Fig. 8a,b). Both independent groups Al-Co-Al seem to be unstable and bent. In the pentagonal environment, there are five different arrangements of the bent Al-Co-Al group in respect to the capped side of the pentagonal antiprism. This yields five different orientations of the three-atomic cavity cap (Fig. 8c). The distances between the cavities within the (100) plane (ca. 6 Å) and between two capes of the same cage along [100] (ca. 8 Å) are quite large (Fig. 8a,b). Thus correlations between the orientation of the triangular caps of the neighboring cages and the opposite caps of the same cage have to be weak. This may be one reason for the translational disorder.

A second reason for the translational disorder may originate from a special kind of stacking faults. The crystal structures of *o*-$Al_{13}Co_4$ and $Al_{13}Fe_4$ (*m*-$Al_{13}Co_4$) are formed by the same kind of cage columns [20]. The difference between both structures is given by the relative orientation of the pairs of columns in the (100) plane: in *o*-$Al_{13}Co_4$ the pairs form a zig-zag pattern (Fig. 9), while in $Al_{13}Fe_4$ all pairs are arranged following a parallel pattern. Such stacking faults are frequently observed in intermetallic compounds. Besides in closest-packed structures, this kind of stacking pattern was shown for a-$TmAlB_4$ (structure type $ThMoB_4$, parallel arrangement of the equivalent fragments) and b-$TmAlB_4$ (structure type $YCrB_4$, zig-zag pattern). In single crystals of both modifications, small segments were found showing the other arrangement with respect to the basic matrix [30-32].

However, such inclusions were not found in the HRTEM images of *o*-$Al_{13}Co_4$. Instead, additional reflections appear in the electron diffraction images of some regions of the investigated crystals in the [010] zone (Fig. 10a) and indicate a doubling of the orthorhombic unit cell with the unit cell size of 16.2 Å × 12.5 Å × 28.8 Å ($2a \times b \times 2c$). However, the extinction conditions for the *h*0*l* reflections are not appropriate assuming an orthorhombic superstructure. General conditions for *h*0*l* reflections for a superstructure may be $h + l = 2n$ corresponding to a possible *n* glide plane or $h = 4n$, or $l = 4n$ for *h*00 or 00*l*, respectively, corresponding to a possible diamond *d* glide plane. In the electron diffraction images of *o*-$Al_{13}Co_4$, the *h*0*l* reflections are systematically absent with $h = 4n + 2$ and $l = 4n$ or with $h = 4n$ and $l = 4n + 2$ (Fig. 10a), which usually points towards presence of twinning. Therefore, such diffraction patterns were interpreted with twinning of a monoclinic unit cell with parameters 18.7 Å ×12.5 Å ×16.5 Å and $\beta \approx 118.5°$, space group *P*2/*c* with *h*0*l*, $l = 2n$ and the twinning plane being (001), cf. Fig. 10b, indicating a more complex structure modification than suggested in [20]. Other monoclinic structures were already reported for $Al_{13}Co_4$, the smallest variant with space group *C*2/*m*, $a = 17.0607$ Å, $b = 4.1063$ Å, $c = 7.5055$ Å, $\beta = 115.247°$ [10], the largest one (t^2-$Al_{13}Co_4$, space group *Pm*, $a = 19.912$ Å, $b = 8.124$ Å, $c = 32.133$ Å, $\beta = 108.042°$ [9]. Further monoclinic types with considerable larger cell sizes, *e.g.*, $a = 39.8$ Å, $b = 8.1$ Å, $c = 39.2$ Å, $\beta = 108°$ were reported at elevated temperatures [13]. However, this kind of structure modification should be examined in detail since sample preparation effects have to be taken into account, as they may result in twinning or superstructure formation [33,34].

CONCLUSIONS

High-resolution TEM, STEM and X-ray diffraction experiments on orthorhombic *o*-$Al_{13}Co_4$ - a quasicrystal approximant - confirmed the symmetry of space group $Pmn2_1$ reported by the first study of the crystal structure. The X-ray diffraction experiments on single-crystals grown via the Bridgman and Czochralski techniques revealed a much more complex model of the crystal structure, which includes multiple split and partially occupied crystallographic sites. The model was confirmed by high-resolution TEM and STEM studies made on focused-ion-beam prepared specimens cut from large single crystals. In agreement with the X-ray diffraction data, the HRTEM and HRSTEM images revealed a structural arrangement with strong local violations of translational symmetry, in particular by aluminum positions located on the mirror plane. Bonding interactions between the three-dimensional framework and three-atomic Co-Al-Co groups located in the cavities of the latter in combination with large distances between the cages and cage caps are one possible reason for the extended disorder. The local twinning in different directions or stacking faults are another possible origin of the experimentally observed crystallographic features.

Acknowledgments

The authors acknowledge Ulrich Schwarz for valuable discussions. The presented and other studies on $Al_{13}Co_4$ referred in the text were performed in cooperation within the European Integrated Centre for the Development of New Metallic Alloys and Compounds (European C-MetAC). The authors appreciate the long-term collaboration with several groups within European C-MetAC.

REFERENCES

1. T. Gödecke. Number and composition of the intermetallic phases in the Al-Co system between 10% and 40% Co. *Z. Metallkd.* 62 (1971) 842-843.
2. A. J. McAlister. The Al-Co (Aluminum-Cobalt) system. *Bull. Alloy Phase Diagrams* 10 (1989) 646-650.
3. M. Ellner, S. Kek and B. Predel. Zur Existenz einer Phase Co_3Al vom Cu_3Au-Strukturtyp. *J. Alloys Compd.* 189 (1992) 245-248.
4. W. Ekman. Strukturanalogien der binären Legierungen von Übergangselementen mit Zn, Cd und Al. *Z. Phys. Chem. B* 12 (1931) 57-58.
5. A. J. Bradley and C. S. Cheng. The crystal structure of Co_2Al_5. *Z. Kristallogr.* 4, 99 (1938) 480-487.
6. J. B. Newkirk, P. J. Black, A. Damjanovic. The refinement of the Co_2Al_5 structures. *Acta Crystallogr.* 14 (1961) 532-533.
7. A. M. B. Douglas. The structure of Co_2Al_9. *Acta Crystallogr.* 3 (1950) 19-24.
8. M. Boström, H. Rosner, Yu. Prots, U. Burkhardt, Yu. Grin. The Co_2Al_9 Structure Type Revisited. *Z. Anorg. Allg. Chem.* 631 (2005) 534-541.
9. U. Burkhardt. Strukturelle und metrische Zusammenhänge von Kristallstrukturen mit pentagonalen Clustern. *PhD Thesis*, Universität Stuttgart (1996).
10. P. Priputen, M. Kusý, M. Drienovský, D. Janickovi, R. Cicka I. Cernickova, J. Janovec. Experimental reinvestigation of Al-Co phase diagram in vicinity of $Al_{13}Co_4$ family of phases. *J. Alloys Compd.* 647 (2015) 486-497.
11. A. Ormeci, Yu. Grin. Chemical Bonding in Al_5Co_2: The Electron Localizability - Electron Density Approach. *Isr. J. Chem.* 51 (2011) 1349-1354.
12. M. Armbrüster, K. Kovnir, Yu. Grin, R. Schlögl. Complex Metallic Alloys: Fundamentals and Applications, Wiley-VCH (2011) 385ff.
13. X. L. Ma, K. H. Kuo, Decagonal quasi-crystal and related crystalline phases in slowly solidified Al-Co alloys. *Metall. Trans. A - Phys. Metall. Mater. Sci.* 23 (1992) 1121-1128.
14. J. Dolinšek, M. Komelj, P. Jeglič, S. Vrtnik, D. Stanić, P. Popčević, J. Ivkov, A. Smontara, Z. Jagličić, P. Gille, Yu. Grin. Anisotropic magnetic and transport properties of orthorhombic $Al_{13}Co_4$. *Phys. Rev. B 79* (2009) 184201.
15. R. Addou, E. Gaudry, Th. Deniozou, M. Heggen, M. Feuerbacher, P. Gille, Yu. Grin, R. Widmer, O. Gröning, V. Fournée, J.-M. Dubois, J. Ledieu. Structure investigation of the (100) surface of the orthorhombic $Al_{13}Co_4$ crystal. *Phys. Rev. B 80* (2009) 014203.

16. R. Addou, A. K. Shukla, S. Alarcon Villaseca, E. Gaudry, Th. Deniozou, M. Heggen, M. Feuerbacher, R. Widmer, O. Gröning, V. Fournee, J.-M. Dubois, J. Ledieu. Lead adsorption on the $Al_{13}Co_4$ (100) surface: heterogeneous nucleation and pseudomorphic growth. *New J. Phys.* 13 (2011) 103011.
17. M. Armbrüster, K. Kovnir, M. Friedrich, D. Teschner, G. Wowsnick, M. Hahne, P. Gille, L. Szentmiklósi, M. Feuerbacher, M. Heggen, F. Girgsdies, D. Rosenthal, R. Schlögl, Yu. Grin. $Al_{13}Fe_4$ as a low-cost alternative for palladium in heterogeneous hydrogenation. *Nature Mater.* 11 (2012) 690-693.
18. R. C. Hudd, W. H. Taylor. Structure of Co_4Al_{13}. *Acta Crystallogr.* 15 (1962) 441-442.
19. X. Z. Li, X. L. Ma, K. H. Kuo. *Collected Abstracts of the XVIth Congress of the IUCr,* Beijing, 1993, p. 342.
20. J. Grin, U. Burkhardt, M. Ellner, K. Peters. Crystal structure of orthorhombic Co_4Al_{13}. *J. Alloys Compd.* 206 (1994) 243-247.
21. M. Heidelmann, M. Heggen, C. Dwyer, M. Feuerbacher. Comprehensive model of metadislocation movement in $Al_{13}Co_4$. *Script. Mater.* 98 (2015) 24-27.
22. P. Gille, B. Bauer. Single crystal growth of $Al_{13}Co_4$ and $Al_{13}Fe_4$ from Al-rich solutions by the Czochralski method. *Cryst. Res. Technol.* 43 (2008) 1161–1167.
23. M. Heggen, L. Houben, M. Feuerbacher. Metadislocations in the orthorhombic structurally complex alloy $Al_{13}Co_4$. *Phil. Mag.* 88 (2008) 2333-2338.
24. M. Heggen, D. Deng, M. Feuerbacher. Plastic deformation properties of the orthorhombic complex metallic alloy phase $Al_{13}Co_4$. *Intermetallics* 15 (2007) 1425-1431.
25. M. Feuerbacher, M. Heggen. On the concept of metadislocations in complex metallic alloys. *Phil. Mag.* 86 (2006) 8985-990.
26. M. Heggen and M. Feuerbacher. Core structure and motion of metadislocations in the orthorhombic structurally complex alloy $Al_{13}Co_4$. *Mat. Res. Lett.* 2 (2014) 145-151.
27. H. D. Flack. On Enantiomorph-Polarity Estimation. *Acta Crystallogr.* A39 (1983) 876–881.
28. H. D. Flack, G. Bernardinelli. The use of X-ray crystallography to determine absolute configuration. *Chirality* 20 (2008) 681-690.
29. P. Jeglic, S. Vrtnik, M. Bobnar, M. Klanjsek, B. Bauer, P. Gille, Yu. Grin, F. Haarmann, J. Dolinsek. M-Al-M groups trapped in cages of $Al_{13}M_4$ (M=Co, Fe, Ni, Ru) complex intermetallic phases as seen via NMR. *Phys. Rev. B* 82 (2010) 104201.
30. T. Mori, H. Borrmann, S. Okada, K. Kudou, A. Leithe-Jasper, U. Burkhardt, Yu. Grin. Crystal structure, chemical bonding, electrical transport, and magnetic behavior of $TmAlB_4$. *Phys. Rev. B* 76 (2007) 064404.

31. K. Yubuta, T. Mori, A. Leithe-Jasper, Yu. Grin, S. Okada, T. Shishido. Direct observation of the intergrown α-phase in β-$TmAlB_4$ via high-resolution electron microscopy. *Mater. Res. Bull.* 44 (2009) 1743-1746.
32. K. Yubuta, T. Mori, A. Leithe-Jasper, H. Borrmann, Yu. Grin, S. Okada, T. Shishido. Intergrowth structure of α-phase in β-type $TmAlB_4$ compound studied by high-angle annular detector dark-field scanning transmission electron microscopy. *J. Solid State Chem.* 219 (2014). 274-279.
33. L. D. Madsen, L. Weaver, S. N. Jacobsen. Influence of Material Properties on TEM Specimen Preparation of Thin Films. *Micr. Res. Tech.* 36 (1997) 354–361.
34. S. B. Rice, M. M. J. Treacy. The Art of the Possible: An Overview of Catalyst Specimen Preparation Techniques for TEM Studies. *115 MRS Symp. Proc.* 15 (1987) 15-27.

Table 1. Crystallographic information on the single crystals of *o*-$Al_{13}Co_4$ investigated.

	Crystal 1	Crystal 2	Crystal 3	Crystal 0 [20]
Composition (refined)	$Co_{24.0}Al_{76.0(4)}$	$Co_{24.0}Al_{76.1(5)}$	$Co_{24.0}Al_{76.0(5)}$	$Co_{24}Al_{76}$
Number of reflections for lattice parameter refinement	203	198	9045	37
a	8.1590(6)	8.1650(5)	8.1650(3)	8.158(1)
b	12.349(1)	12.3500(8)	12.3520(6)	12.342(1)
c	14.453(1)	14.449(1)	14.4598(7)	14.452(2)
Number of reflections measured	31104	18899	26122	1948
Number of reflections unique	8979	8391	4669	1948
R_{int}	0.035	0.035	0.043	-
Number of reflections with $\lvert I \rvert > 3\sigma I$	5949	4860	3650	854
Number of refined parameters	340	268	269	268
Flack parameter	0.32(2)	0.24(6)	0.13(2)	-
GOF	1.05	0.91	1.06	-
R_F	0.035	0.039	0.041	0.062

Table 2. Atomic coordinates and equivalent displacement parameters (in Å^2) in the crystal structure of *o*-$Al_{13}Co_4$ (crystals 1 and 2)*. The list of anisotropic ADPs can be obtained from the authors.

Atom	Site	Occupancy	*x*	*y*	*z*	U_{eq}
Co1	2*a*		0	0.8989(2)	0.0**	0.0058(5)
			0	0.8970(1)	0.0**	0.0056(3)
Co2	2*a*		0	0.0887(2)	0.5130(2)	0.0060(5)
			0	0.0880(1)	0.5141(1)	0.0058(3)
Co3	2*a*		0	0.2045(2)	0.8206(2)	0.0069(5)
			0	0.2065(1)	0.8219(1)	0.0058(3)
Co4	2*a*		0	0.7703(2)	0.3131(2)	0.0065(5)
			0	0.7704(1)	0.3129(1)	0.0048(3)
Co5	2*a*		0	0.6006(2)	0.8269(1)	0.0082(5)
			0	0.5993(1)	0.8263(1)	0.0071(3)
Co6	2*a*		0	0.4125(2)	0.3140(2)	0.0061(5)
			0	0.4105(1)	0.3149(1)	0.0033(2)
Co7	2*a*		0	0.7297(2)	0.5143(2)	0.0042(4)
			0	0.7304(1)	0.5140(1)	0.0066(3)
Co8	2*a*		0	0.2952(2)	0.0046(2)	0.0054(5)
			0	0.2969(1)	0.0061(1)	0.0058(3)
Co9	4*b*	0.89(3)	0.2199(5)	0.9066(5)	0.7318(5)	0.0069(7)
		0.89(5)	0.2228(1)	0.9062(1)	0.7311(1)	0.0056(3)
Co9a	4*b*	0.13***	0.250(3)	0.913(3)	0.728(3)	0.0040(3)
		0.11	0.2353(9)	0.9153(6)	0.7243(5)	0.0058(5)
Co10	4*b*	0.67(2)	0.2334(4)	0.5924(5)	0.0945(5)	0.0049(7)
		0.62(2)	0.2337(2)	0.5916(1)	0.0935(1)	0.0052(2)
Co10a	4*b*	0.33	0.1977(10)	0.5900(11)	0.0965(10)	0.0084(12)
		0.38	0.2022(3)	0.5907(2)	0.0957(2)	0.0069(3)
Al1	2*a*	0.61(1)	0	0.9964(8)	0.8224(7)	0.013(2)
		0.43(2)	0	0.9968(5)	0.8115(6)	0.009(2)
Al2	2*a*	0.80(1)	0	0.0929(10)	0.9608(6)	0.0122(14)
		0.84(5)	0	0.0913(3)	0.9586(3)	0.0090(7)
Al2a	2*a*	0.20	0	0.096(4)	0.982(2)	0.009(2)
		0.16	0	0.096(2)	0.973(1)	0.0095(6)
Al3	2*a*		0	0.9046(5)	0.6184(4)	0.0129(12)
			0	0.9007(3)	0.6184(2)	0.0109(7)
Al4	2*a*		0	0.9114(5)	0.4360(4)	0.0088(10)
			0	0.9128(3)	0.4351(2)	0.0093(7)
Al5	2*a*	0.74(2)	0	0.1210(7)	0.6741(6)	0.008(2)

		0.88(2)	0	0.1174(3)	0.6754(3)	0.0110(4)
Al5a	2*a*	0.26	0	0.153(2)	0.660(2)	0.011(4)
		0.12	0	0.154(2)	0.659(2)	0.0097(6)
Al6	2*a*	0.55(3)	0	0.8037(14)	0.1501(15)	0.010(3)
		0.49(3)	0	0.8033(5)	0.1493(4)	0.0082(5)
Al6a	2*a*	0.45	0	0.829(2)	0.156(2)	0.011(4)
		0.51	0	0.8306(5)	0.1582(4)	0.0086(5)
Al7	2*a*	0.48(2)	0	0.8005(6)	0.8416(6)	0.0101(11)
		0.47(2)	0	0.7989(5)	0.8463(5)	0.0098(5)
Al7a	2*a*	0.29(1)	0	0.8466(9)	0.8289(6)	0.010(2)
		0.42(2)	0	0.8467(6)	0.8288(5)	0.0105(5)
Al8	2*a*		0	0.2481(6)	0.4151(5)	0.0092(11)
			0	0.2478(5)	0.4159(5)	0.0079(5)
Al9	2*a*		0	0.4001(4)	0.8528(5)	0.0114(12)
			0	0.4001(3)	0.8501(2)	0.0107(7)
Al10	2*a*	0.53(1)	0	0.3630(8)	0.1596(7)	0.006(2)
		0.67(2)	0	0.3598(4)	0.1597(3)	0.0066(5)
Al10a	2*a*	0.47	0	0.4037(8)	0.1427(8)	0.010(2)
		0.33	0	0.4077(8)	0.1404(6)	0.0105(6)
Al11	2*a*	0.48(5)	0	0.674(6)	0.672(6)	0.010(8)
		0.40(10)	0	0.6781(6)	0.6706(5)	0.0068(5)
Al11a	2*a*	0.52	0	0.692(5)	0.677(5)	0.008(6)
		0.60	0	0.6878(4)	0.6767(4)	0.0086(5)
Al12	2*a*		0	0.5890(4)	0.3911(4)	0.0092(11)
			0	0.5893(3)	0.3895(2)	0.0072(6)
Al13	2*a*	0.44(1)	0	0.5430(9)	0.0098(8)	0.023(2)
		0.41(2)	0	0.5392(7)	0.0079(6)	0.0155(6)
Al13a	2*a*	0.56	0	0.4970(9)	0.0155(8)	0.017(2)
		0.59	0	0.4968(4)	0.0094(4)	0.0107(5)
Al14	2*a*		0	0.5958(4)	0.2098(5)	0.0129(12)
			0	0.5918(3)	0.2093(3)	0.0117(7)
Al15	4*b*		0.2172(5)	0.2059(3)	0.0969(3)	0.0083(3)
			0.2139(3)	0.2054(2)	0.0954(2)	0.0079(4)
Al16	4*b*		0.2183(5)	0.9090(3)	0.2842(3)	0.0092(8)
			0.2251(3)	0.9075(2)	0.2870(2)	0.0100(4)
Al17	4*b*		0.2324(5)	0.0814(3)	0.4041(3)	0.0115(8)
			0.2335(3)	0.0821(2)	0.4043(2)	0.0098(5)
Al18	4*b*		0.2497(2)	0.2498(4)	0.9129(4)	0.0077(3)
			0.2499(2)	0.2515(4)	0.9144(4)	0.0071(3)
Al19	4*b*		0.2202(5)	0.9830(3)	0.0914(3)	0.0089(8)

			0.2211(3)	0.9807(2)	0.0903(2)	0.0075(4)
Al20	4*b*		0.2280(5)	0.2240(3)	0.5454(3)	0.0125(9)
			0.2295(3)	0.2232(2)	0.5463(2)	0.0087(5)
Al21	4*b*		0.2202(6)	0.5916(3)	0.5428(3)	0.0133(9)
			0.2142(3)	0.5902(2)	0.5449(2)	0.0105(5)
Al22	4*b*		0.2187(4)	0.2934(3)	0.7287(3)	0.0076(8)
			0.2210(3)	0.2938(2)	0.7277(2)	0.0070(4)
Al23	4*b*		0.2320(4)	0.4198(3)	0.4220(3)	0.0077(3)
			0.2315(3)	0.4218(2)	0.4217(2)	0.0076(4)
Al24	4*b*		0.2211(4)	0.5182(3)	0.7355(3)	0.0087(8)
			0.2200(3)	0.5157(2)	0.7343(2)	0.0088(4)
Al25	4*b*		0.2265(5)	0.2775(3)	0.2804(3)	0.0088(7)
			0.2260(3)	0.2762(2)	0.2813(2)	0.0119(5)
Al26	2a	0.24(1)	0	0.7387(9)	0.9270(8)	0.010(6)
		0.21(3)	0	0.738(1)	0.927(1)	0.0108(6)
Al26a	2*a*	0.33(2)	0	0.6867(10)	0.9892(7)	0.010(2)
		0.35(2)	0	0.6893(7)	0.9907(6)	0.0105(6)
Al26b	2*a*	0.24(1)	0	0.7170(10)	0.9571(11)	0.010(4)
		0.23(2)	0	0.718(1)	0.9521(9)	0.0105(6)
Al27	2*a*		0	0.0928(6)	0.2408(5)	0.017(2)
			0	0.0920(3)	0.2417(3)	0.0125(4)
Al28	2*a*		0	0.4056(5)	0.5905(5)	0.0168(13)
			0	0.4046(3)	0.5915(3)	0.0156(8)

* The lines with an atom identifier contain information from the crystal one. The lines without atom identifier contain information about the equivalent positions from the crystal 2.

** Fixed for the refinement.

*** Occupancy parameters refined with a constraint to 1 are given without estimated standard deviations (e.s.d.), all other occupancy parameters were refined independently.

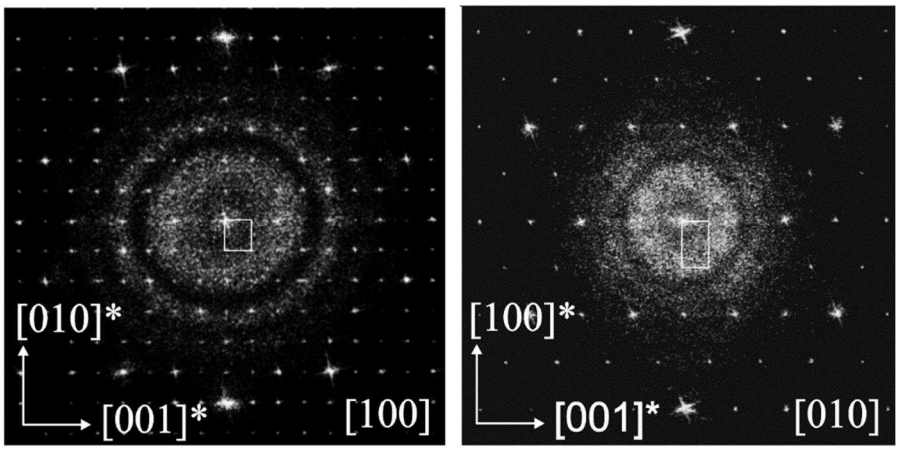

Figure 1. Characteristic FFTs of HRTEM images (equivalent to local electron diffraction patterns) of *o*-$Al_{13}Co_4$ (crystal 1) along the [100] and [010] directions with the projections of the unit cell (reciprocal space).

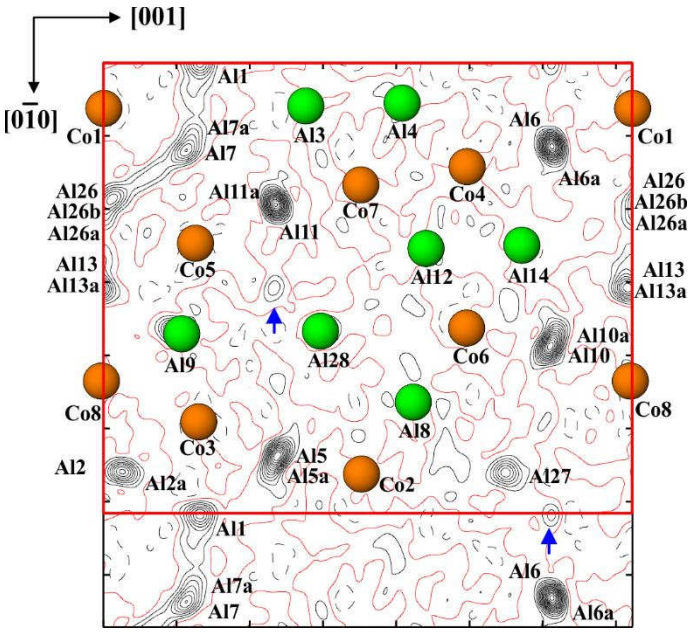

Figure 2. Difference electron density of *o*-$Al_{13}Co_4$ in the (100) plane (crystal 1) calculated without split positions. Isolines are drawn with a step of 5 e $Å^{-3}$, positive levels – black solid lines, zero level red solid line, negative levels – black dashed lines. Non-identified maxima are marked by blue arrows.

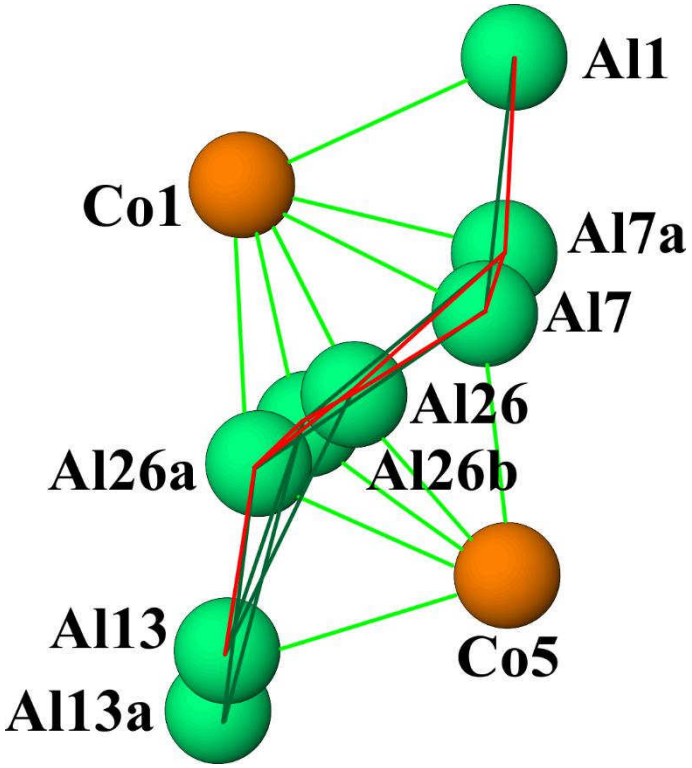

Figure 3. Interatomic distances in the vicinity of Al7 atom in the (100) plane. The distances larger than 2.2 Å are shown in green (light green for Co-Al, dark green for Al-Al distances), the distances smaller than 2.2 Å are drawn in red.

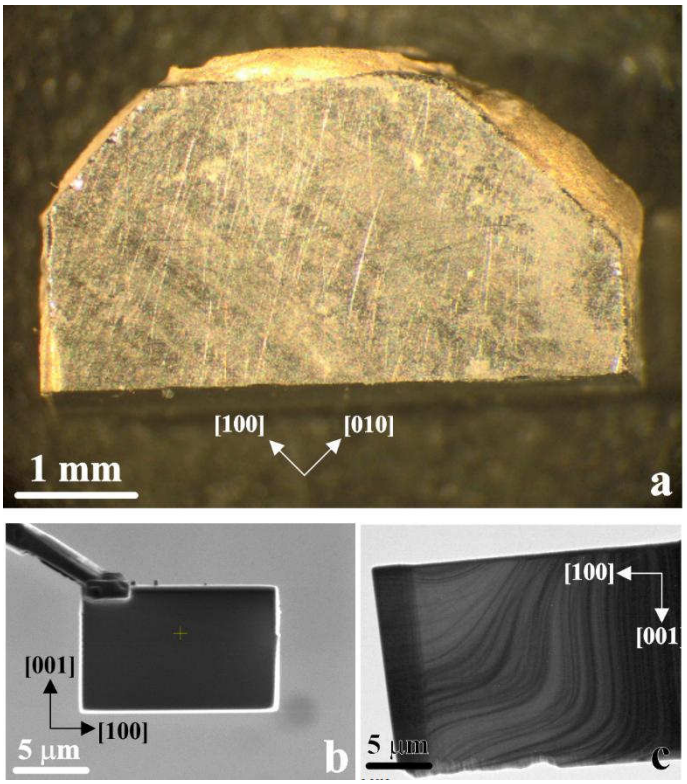

Figure 4. (a) Light microscopy of the single crystal grown by the Czochralski method. (b) Focused ion beam lift-out lamella, SEM image. (c) TEM image of FIB cut showing traces of argon milling giving rise to steps.

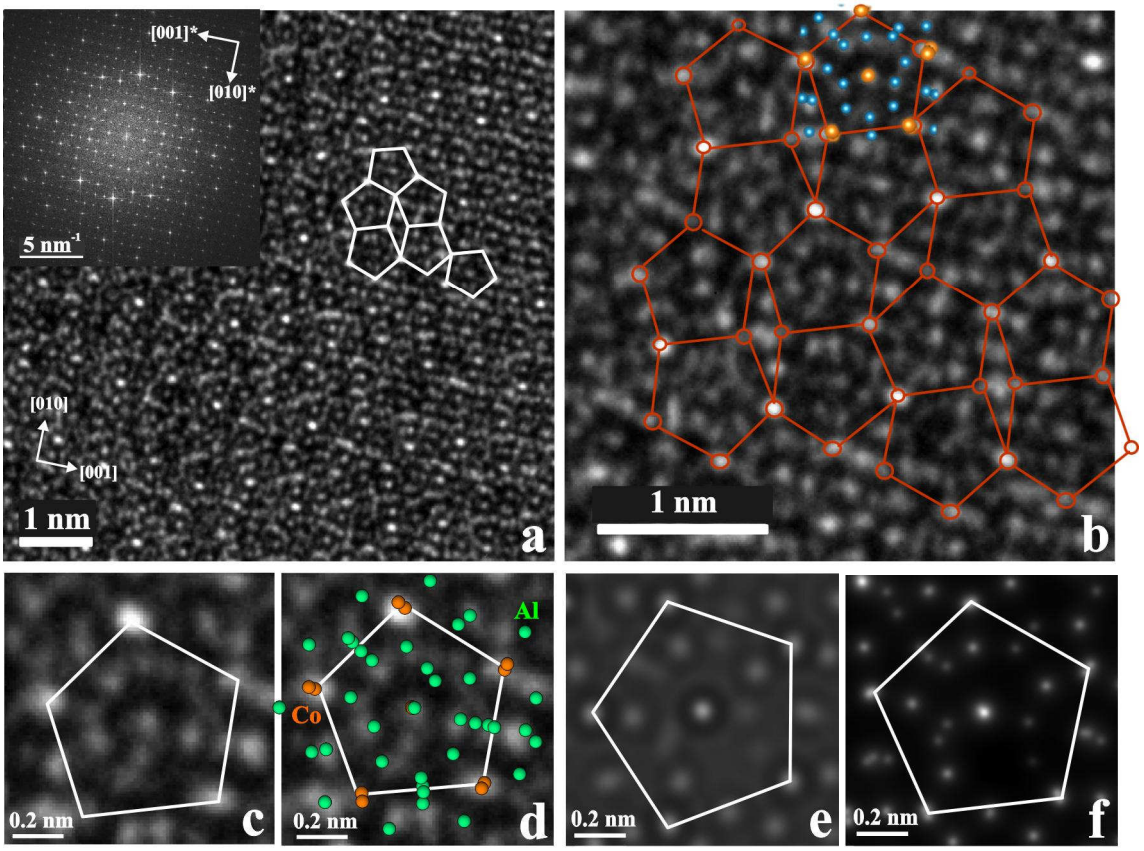

Figure 5. Transmission electron microscopy (HRTEM, 300 kV acceleration voltage) of [100] zone in *o*-$Al_{13}Co_4$. (a) Overview image. The bright spots mark the cobalt-containing columns situated at the corners of the pentagon. The inset shows a FFT with the typical pseudo 10-fold symmetry. (b) Magnified area from (a) with overlaid model of disorder of Al atoms (blue) within the pentagonal pattern. Large pentagons correspond to Co-containing columns. (c-f) Experimental (c,d) and calcualted (e,f) large-scale image without (c) and with (d) overlay of a disordered model (Co – orange, Al – green); (f) Projected Coulomb potential image of the nuclei visualizing atomic positions.

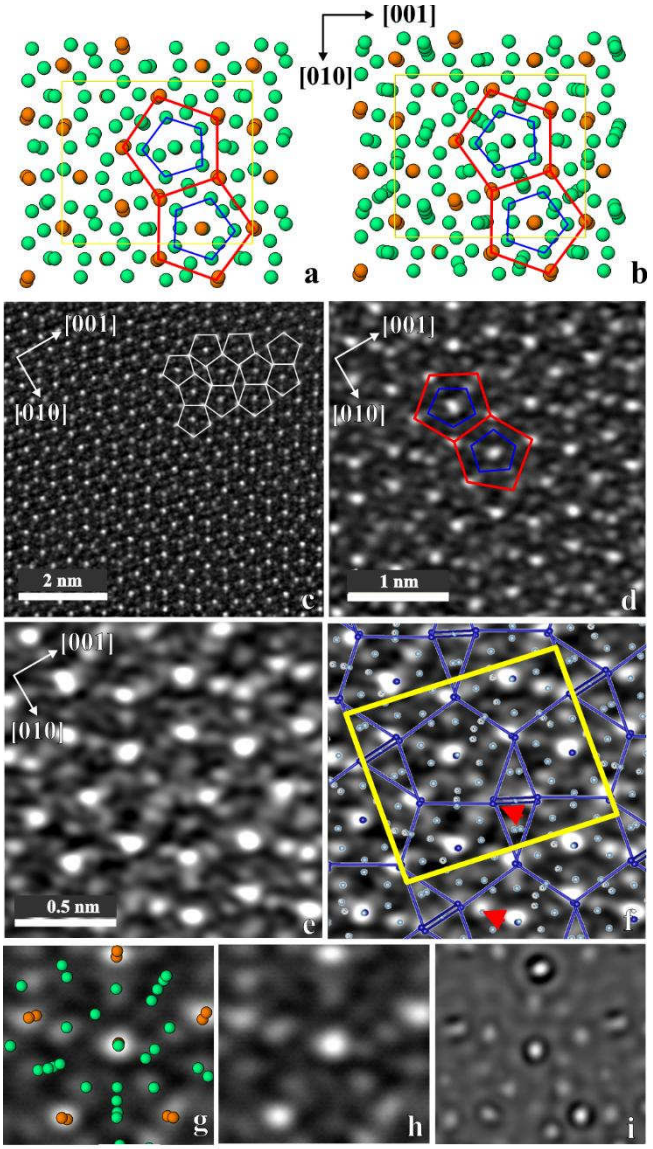

Figure 6. Scanning transmission electron microscopy of *o*-$Al_{13}Co_4$ (HRSTEM) in the [100] zone: (a,b) Projections of the ordered and disorder models, respectively, along the [100] direction (Co - orange, Al - green). (c) STEM overview image of [100] zone. (d) Micrograph at higher magnification with model overlaid comprising 5 Co atoms (red) in the neighboring pentagons and the corresponding 5 inner Al atoms (blue). (e,f) STEM image without (e) and with (f) overlaid model displaying pentagonal network of Co (blue) and disordered Al atoms (light blue); unit cell marked by yellow rectangle; some Co atoms at the corners of the pentagon are less pronounced (red arrows) due to the zig-zag formation of Co along the view direction or due to a lack of atoms in the column. (g,h,i) Selected part of the image (e) with (g) and without (h) overlaid disordered model (Co – orange, Al – green) and its simulation (i).

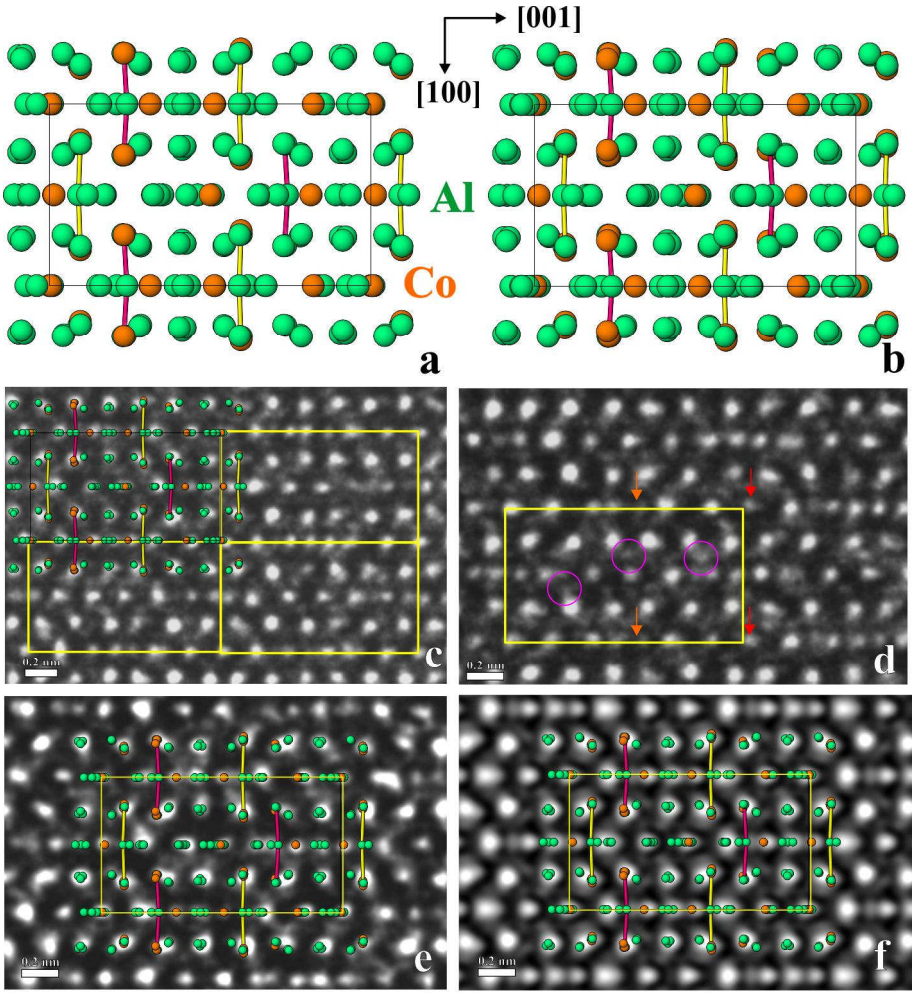

Fig. 7. HRTEM of *o*-$Al_{13}Co_4$ along the [010] direction: (a,b) In projection along [010], there is not a large difference between the model with all split positions (a) and the ordered model (b). (c) Overview image with four unit cells (yellow). The model of disordered structure is overlaid indicating the appearance of four layers along [100]. (d) Other regions show different splitting at the corners and central positions of the first and fifth layer, see red and orange arrows, besides the interstitial positions (pink circles). (e) The Co-Al-Co groups in the presented region (Co10-Al28-Co10 - yellow and Co9-Al27-Co9 - pink). (f) FFT-filtered image, aluminum atoms from the yellow dumbbell are resolved, aluminum from the violet dumbbell is situated near an atomic column with strong intensity and thus these two positions are merged in one spot which cannot be resolved.

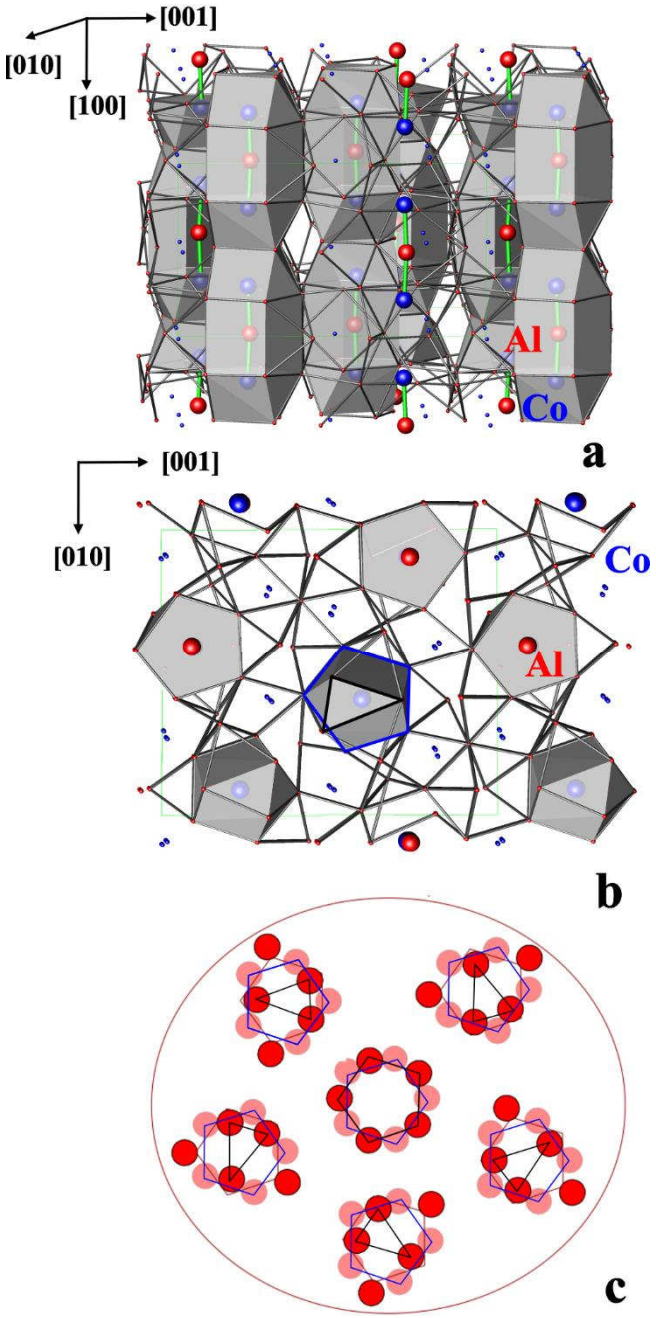

Fig. 8. Chemical bonding as the reason for the disorder in the crystal structure of *o*-$Al_{13}Co_4$. (a) Cages in the three-dimensional framework. (b) Projection of the crystal structure along [100]. (c) Scheme of five possible orientations of the cage caps, in respect to the pentagonal-prismatic part of a cage, caused by different location of the Co-Al-Co groups within the cages.

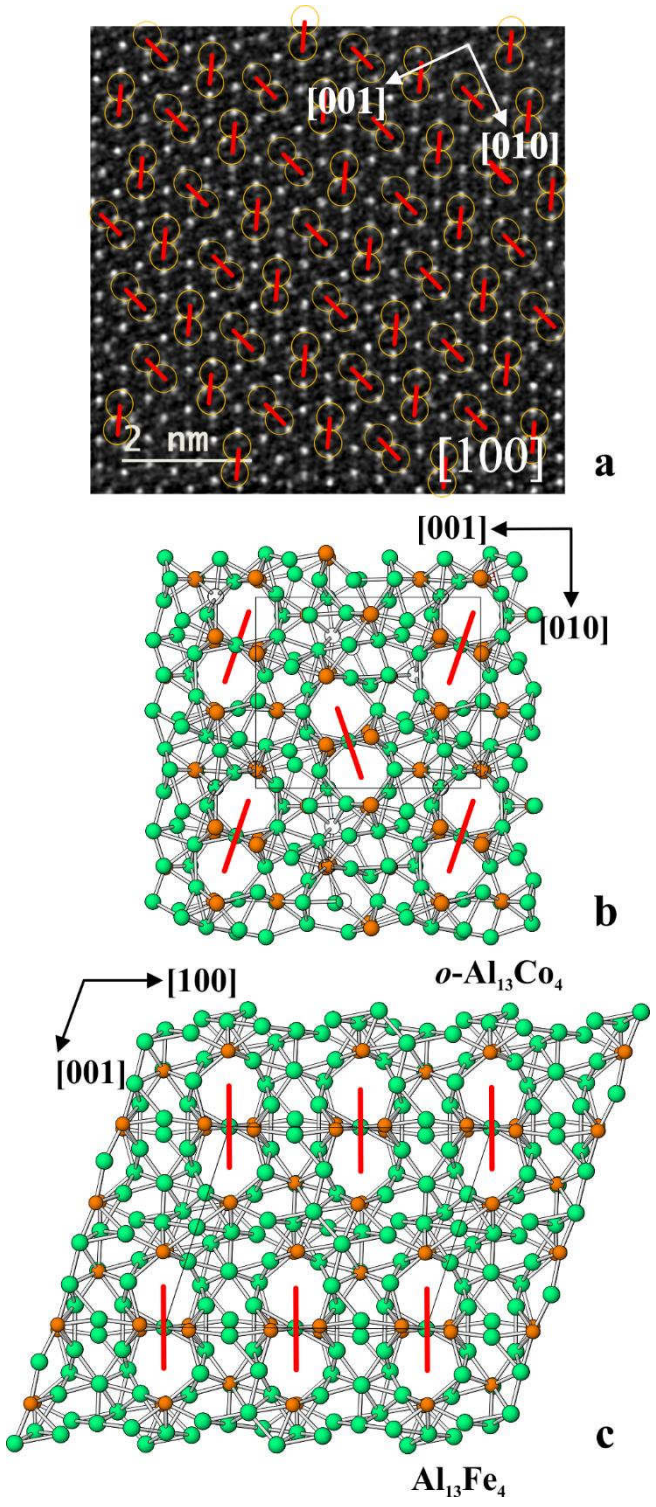

Fig. 9. Segment stacking in *o*-$Al_{13}Co_4$ (STEM image, a) and the scheme of the stacking in the related structures of *o*-$Al_{13}Co_4$ and $Al_{13}Fe_4$ [20] (b, c).

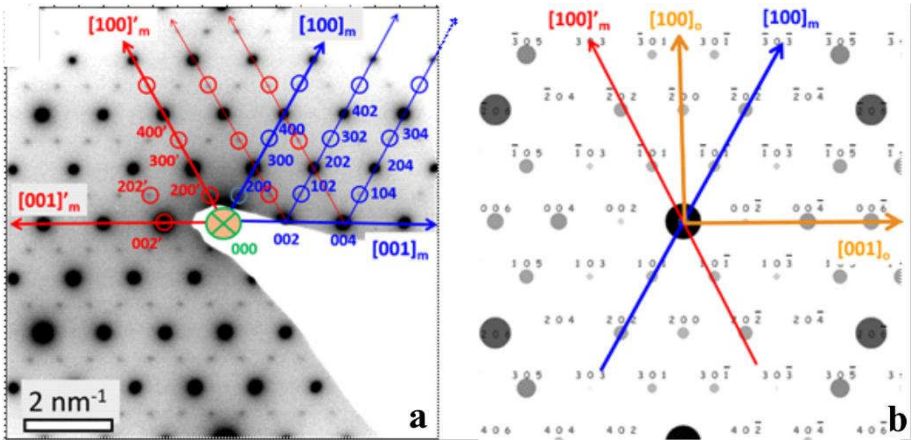

Fig. 10. (a) Electron diffraction image of *o*-$Al_{13}Co_4$ ([010] zone) with periodicity doubling ($2a \times b \times 2c$) giving rise to a new monoclinic structural pattern. Two monoclinic domains are indicated in red and blue with a twinning angle of 118.5°. (b) Simulated pattern of [010] zone with the new unit cell axes (red and blue).